

**NASA Technical Memorandum 56049**

**Buffet Characteristics of  
the F-8 Supercritical Wing Airplane**

**V. Michael DeAngelis and Richard C. Monaghan**

**SEPTEMBER 1977**



**NASA Technical Memorandum 56049**

**Buffet Characteristics of  
the F-8 Supercritical Wing Airplane**

**V. Michael DeAngelis and Richard C. Monaghan**

**Dryden Flight Research Center**

**Edwards, California**



**National Aeronautics  
and Space Administration**

**Scientific and Technical  
Information Office**

**1977**

# BUFFET CHARACTERISTICS OF THE F-8 SUPERCRITICAL WING AIRPLANE

V. Michael DeAngelis and Richard C. Monaghan  
Dryden Flight Research Center

## INTRODUCTION

An extensive research study has been undertaken on a relatively new wing concept known as the supercritical wing. This wing is designed to delay the onset of the transonic drag rise and thereby significantly improve the cruise performance of subsonic aircraft. These performance gains have been demonstrated in wind tunnel and flight investigations of a modified F-8 airplane (fig. 1). Some flight test results, including correlation to wind tunnel data, are presented in references 1 to 4.

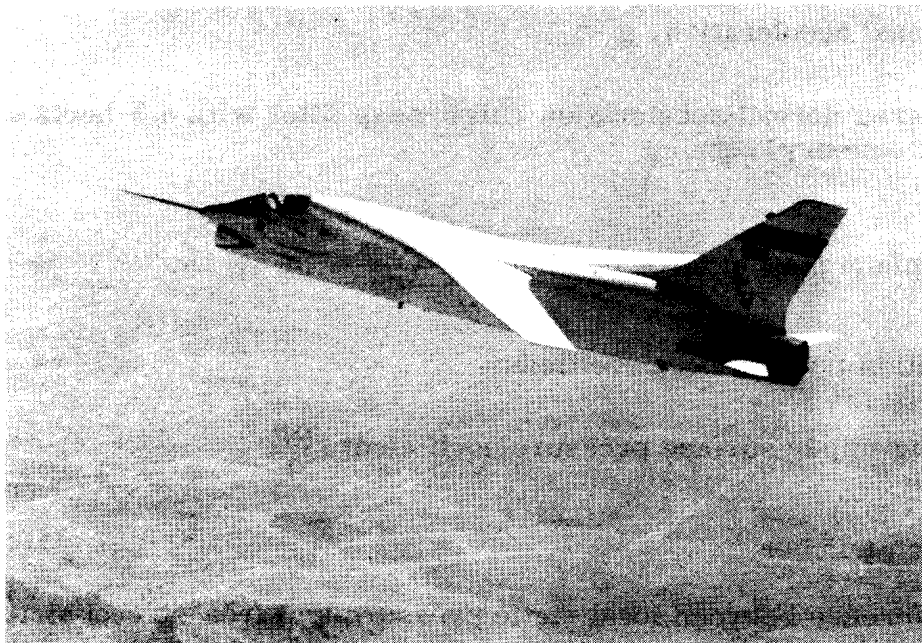


*Figure 1. F-8 supercritical wing airplane.*

Wing pressure measurements demonstrated the supercritical wing's unique ability to maintain an aft shock on the upper surface beyond the normal force coefficient or angle of attack for flow separation. This feature of the upper surface flow held promise for expansion of the buffet-free flight envelope at transonic speeds. To evaluate these potential improvements, airplane and wing structural responses were measured at the pilot station, center of gravity, wing root, wingtip, and aileron during the F-8 supercritical wing flight research program. In addition, a high-frequency dynamic pressure sensor was located in the vicinity of the shock wave that formed on the upper surface of the outer wing panel during transonic flight.

Wing structural response was used to determine the buffet characteristics of the wing. These data are compared with wind tunnel model data and the wing flow characteristics at transonic speeds.

The wing flow characteristics were determined from wind tunnel and flight static pressure distribution data and from flight dynamic pressure data. A flight-determined buffet onset boundary is presented for the Mach number range of 0.50 to 0.99 and includes the effect of moderate trailing edge flap deflections.

## NOMENCLATURE

Physical quantities in this report are given in the International System of Units (SI) and parenthetically in U.S. Customary Units. The measurements were taken and the calculations were made in U.S. Customary Units. Factors relating the two systems are presented in reference 5.

|              |  |
|--------------|--|
| $a_n$        | normal acceleration, g   |
| $\Delta a_n$ | filtered normal acceleration (high-pass filter with a 3-hertz cutoff frequency), g                             |
| $C_{N_A}$    | airplane normal force coefficient, $\frac{a_n W}{qS}$  |
| $c_n$        | section normal force coefficient   |
| $c_{p_u}$    | wing upper surface pressure coefficient, $\frac{\Delta p}{q}$  |
| $M$          | Mach number  |
| $\Delta p$   | difference between local static pressure and free-stream static pressure, $\text{N/m}^2$ (lb/ft <sup>2</sup> ) |
| $q$          | free-stream dynamic pressure, $\text{kN/m}^2$ (lb/ft <sup>2</sup> )  |

|              |   |
|--------------|---|
| rms          | root mean square                                    |
| $S$          | wing reference area, $\text{m}^2$ ( $\text{ft}^2$ ) |
| $W$          | airplane weight, kN (lb)                            |
| $x/c$        | chordwise distance normalized to local chord length |
| $\alpha$     | airplane angle of attack, deg                       |
| $\delta_f$   | wing flap position, deg                             |
| $\delta_h$   | horizontal stabilizer position, deg                 |
| $\epsilon_A$ | aileron hinge strain, m/m (in/in)                   |
| $\epsilon_w$ | wing panel bending strain, m/m (in/in)              |
| $\sigma$     | root mean square value of associated quantity       |
| $\Phi$       | power spectral density of associated quantity       |
| Subscript:   |   |
| $cg$         | center of gravity                                   |

## FLIGHT TEST AIRPLANE

### General Description

The F-8 supercritical wing airplane used in these tests was a modified TF-8A airplane. The original low aspect ratio, thin, fighter-type wing was replaced with a high aspect ratio, moderately thick, transport-type wing that incorporated the most recently developed supercritical wing sections. The research airplane, shown in figure 1, had a design gross weight of approximately 110 kilonewtons (25,000 pounds).

The supercritical wing consisted of a primary wing structure and a forward fairing, termed a glove, that extended from the front beam of the carrythrough box to the cockpit canopy. Fuselage fairings were installed on the rear portion of the fuselage, extending from behind the wing carrythrough box to the midroot chord of the vertical stabilizer. Side fairings were eventually installed on the fuselage beneath the wing and the cockpit canopy for improved area ruling (ref. 6). All structural response data presented in this report were obtained before the side fairings were installed, but some of the flight pressure data were obtained with the side fairings on. However, the presence of the side fairings does not affect the

data correlation made in this report. The supercritical wing was installed with a root incidence angle of  $1.5^\circ$  and approximately  $5^\circ$  of twist, or washout, between the root and tip chords. A vortex generator (ref. 7) was installed on the lower surface of the leading edge of each wing to alleviate a pitchup condition.

### Structural Composition

Figure 2 shows a planform view of the supercritical wing. The wing is a two-cell, three-spar aluminum structure with attached leading and trailing edges.

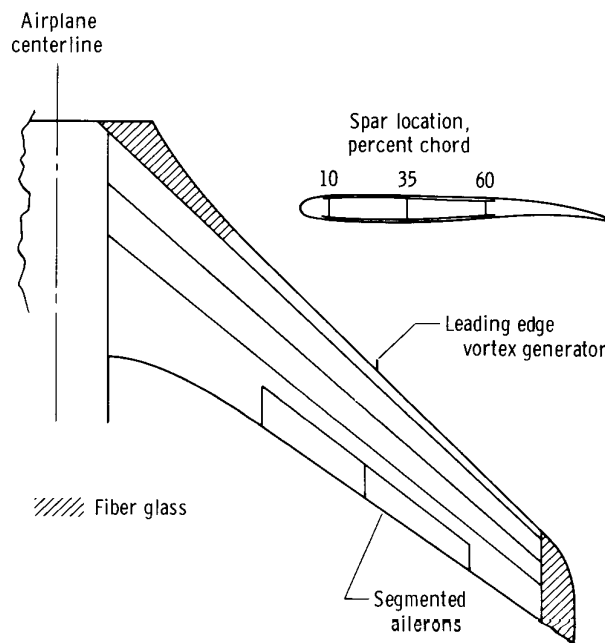


Figure 2. Schematic of wing construction.

The wingtips and portions of the inboard leading edge are constructed of fiber glass. The segmented aluminum ailerons are mechanically connected and are driven by a common actuator. The ailerons, which are hinged at the 75-percent chord, extend from 40 percent of the semispan to 80 percent of the semispan and can be drooped to  $15^\circ$  for takeoff and landing. The geometric characteristics of the wing planform are presented in table 1. Wing section contour coordinates are given in reference 6.

A strict structural design requirement evolved for the supercritical wing. Wind tunnel tests were conducted to develop and optimize the airplane's design. To conduct the tests at the highest possible Reynolds number, the wind tunnel was operated at a dynamic pressure of approximately  $45 \text{ kN/m}^2$  ( $950 \text{ lb/ft}^2$ ). From these tests (ref. 8), the design cruise condition for the wind tunnel model was determined

TABLE 1.—GEOMETRIC CHARACTERISTICS OF  
F-8 SUPERCRITICAL WING

|  |           |               |
|--|-----------|---------------|
| Wing planform, defined by extending the straight-lined leading and trailing edges to the centerline of the fuselage— |           |               |
| Area, m <sup>2</sup> (ft <sup>2</sup> )  | . . . . . | 25.51 (274.5) |
| Span, m (in.)  | . . . . . | 13.14 (517.4) |
| Root chord, m (in.)  | . . . . . | 2.84 (111.9)  |
| Tip chord, m (in.)   | . . . . . | 1.04 (40.9)   |
| Aspect ratio   | . . . . . | 6.773         |
| Taper ratio  | . . . . . | 0.3656        |
| Mean aerodynamic chord, m (in.)  | . . . . . | 2.08 (81.9)   |
| 25-percent chord sweepback angle, deg  | . . . . . | 42.3          |
| 35-percent chord sweepback angle, deg  | . . . . . | 41.4          |
| Aileron planform, both segments—   |           |               |
| Hinge line location, percent chord of wing planform  | . . . . . | 75            |
| Inboard edge location, percent semispan of wing planform   | . . . . . | 40            |
| Outboard edge location, percent semispan of wing planform  | . . . . . | 80            |
| Area, m <sup>2</sup> (ft <sup>2</sup> )  | . . . . . | 1.16 (12.5)   |
| Span, m (in.)  | . . . . . | 2.63 (103.5)  |
| Average chord, m (in.)   | . . . . . | 0.44 (17.3)   |

to be a Mach number of 0.99, a lift coefficient of 0.40, and a wind tunnel dynamic pressure of 44.2 kN/m<sup>2</sup> (923 lb/ft<sup>2</sup>). The design cruise configuration of the wing—that is, the shape of the wing due to aeroelastic deformation at the design cruise condition—was also determined from the wind tunnel tests. At design cruise, the shape of the full-scale airplane wing was required to conform to the shape of the wind tunnel model wing. As a result, the design cruise condition of the full-scale airplane was a Mach number of 0.99, a lift coefficient of 0.40, and a dynamic pressure of 9.6 kN/m<sup>2</sup> (200 lb/ft<sup>2</sup>). The wind tunnel equivalent dynamic pressure is 44.2 kN/m<sup>2</sup> (923 lb/ft<sup>2</sup>). Because the scaled stiffness distribution of the wind tunnel model is similar to that of the flight test airplane, the scaled dynamic pressure relationship between wind tunnel and flight as established for Mach 0.99 should be reasonably valid for most Mach numbers.

Laboratory load tests were conducted to verify that the airplane wing would deform to the proper shape when subjected to the design cruise load distribution. The results of the load tests (ref. 9) indicated that the design requirement was satisfied.

## INSTRUMENTATION AND ACCURACIES

The supercritical wing was instrumented with several sensors, which permitted evaluation of the buffet onset characteristics.

Figure 3 shows the type and location of the buffet instrumentation used in the study. Accelerometers were located at the wingtips, at the pilot compartment,

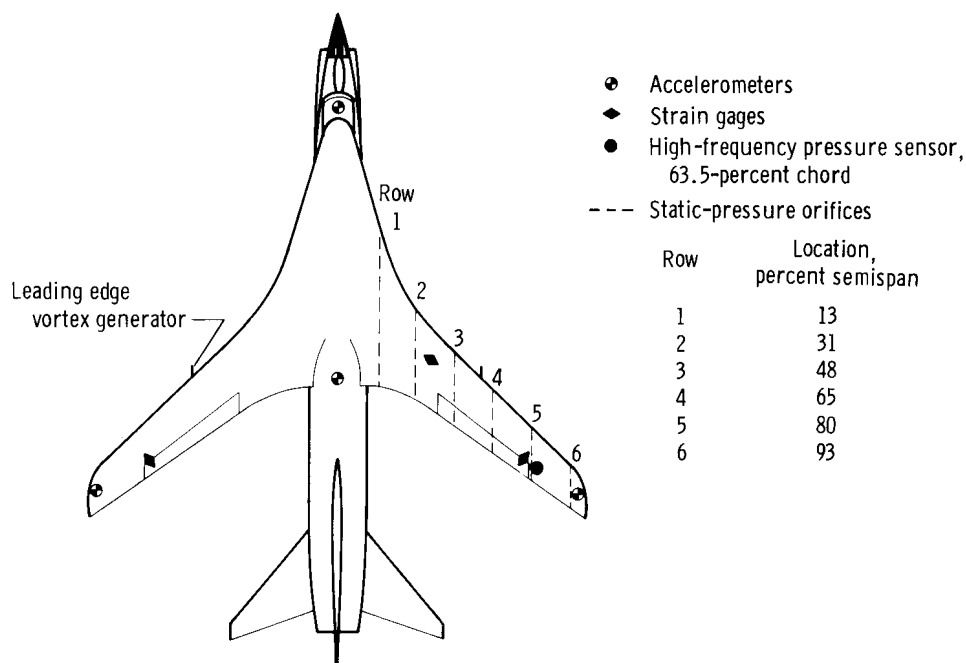


Figure 3. Buffet instrumentation.

and near the center of gravity of the airplane. Strain gages were installed in the right wing panel to measure unsteady bending moments and in the outboard aileron segments to measure unsteady aileron hinge moments.

The signals from the wingtip accelerometers were band-pass filtered to provide data from 3 hertz to 40 hertz. The signals from the wing-panel strain gage and the fuselage accelerometers were low-pass filtered at a frequency of 40 hertz. The aileron strain gage signal was not filtered.

To measure fluctuating pressures, a high-frequency pressure sensor was installed on the upper surface of the right wing panel at the outboard end of the aileron near the hinge line. The sensor was near the position of the aft shock at Mach 0.99 as determined from the wind tunnel data of reference 6. Two hundred and forty-eight flight wing-surface pressure orifices were in six rows on the right wing panel as shown in figure 3. The placement of these pressure orifices is described in detail in reference 4.

The pressure orifices and strain gages used to measure wing-panel bending moment on the flight vehicle were the same as those used on the wind tunnel model.

A compensated pitot-static probe was used to determine Mach number and altitude during the test flights. This airspeed probe was designed at the NASA Langley Research Center to compensate for the Mach number position error of this particular airplane. Reference 10 contains additional discussion of the compensated probe, including the position correction determined from flight tests. The compensated

probe, which included angle of attack and angle of sideslip vanes, was mounted on a nose boom. The angle of attack data were corrected for the effects of local upwash and inertia.

To determine the accuracy of the angle of attack measurement, the longitudinal acceleration was measured accurately during steady state flight. This analysis identified two zero-shift errors, one associated with the angle of sideslip vane and one that existed when the sideslip vane was removed. With the angle of sideslip vane installed, the zero shift appeared to be associated with a shock impingement at transonic speeds and was nonlinear with change in angle of attack. With the sideslip vane removed, the zero shift appeared to be constant with change in angle of attack and Mach number. Therefore, flight data obtained with the sideslip vane are not presented as a function of angle of attack and all flight data obtained without the sideslip vane incorporate a  $0.6^\circ$  angle of attack correction.

A low-pass-filtered normal accelerometer was located at the airplane's center of gravity and was used to determine the airplane normal force coefficient,  $C_{N_A}$ .

Control position transducers were used to measure aileron deflection and horizontal stabilizer position.

Flight data were obtained with a pulse code modulation (PCM) data acquisition system, which provided both onboard tape recording and telemetry for recording at a ground station. The digitized PCM data were sampled at a rate of 200 samples per second and then converted to engineering units.

The estimated errors of the measured quantities used in this report are:

|  |           |                          |
|--|-----------|--------------------------|
| $a_n$ , g                                  | . . . . . | $\pm 0.02$               |
| $C_{N_A}$                                  | . . . . . | $\pm 0.01$               |
| $c_{p_u}$                                  | . . . . . | $\pm 0.01$               |
| $M$  | . . . . . | $\pm 0.003$              |
| $q$ , $\text{kN/m}^2$ ( $\text{lb/ft}^2$ ) | . . . . . | $\pm 0.06$ ( $\pm 1.3$ ) |
| Strain gage output, m/m and in/in          | . . . . . | $\pm 10 \times 10^{-6}$  |
| $\alpha$ , deg                             | . . . . . | $\pm 0.25$               |
| $\delta_f$ , deg                           | . . . . . | $\pm 0.20$               |
| $\delta_h$ , deg                           | . . . . . | $\pm 0.20$               |

## FLIGHT TEST CONDITIONS

A constant dynamic pressure flight envelope was flown; that is, flight data were obtained at different Mach numbers and altitudes for constant dynamic pressures of  $9.6 \text{ kN/m}^2$ ,  $19 \text{ kN/m}^2$ , and  $29 \text{ kN/m}^2$  ( $200 \text{ lb/ft}^2$ ,  $400 \text{ lb/ft}^2$ , and  $600 \text{ lb/ft}^2$ ). However, at a dynamic pressure of  $19 \text{ kN/m}^2$  ( $400 \text{ lb/ft}^2$ ), penetration into buffet beyond

the onset boundary was not possible because of the airplane's load factor limit of 4.0g. At a dynamic pressure of  $29 \text{ kN/m}^2$  ( $600 \text{ lb/ft}^2$ ), the airplane's load factor limit was attained prior to buffet onset. Therefore, all data presented herein were obtained at a dynamic pressure of  $9.6 \text{ kN/m}^2$  ( $200 \text{ lb/ft}^2$ ). Mach number varied from 0.50 to 1.20. Reynolds number varied from  $15 \times 10^6$  to  $24 \times 10^6$ , based on a mean aerodynamic chord of 2.08 meters (81.9 inches). The flight data were obtained from pushover-pullup and windup-turn maneuvers that resulted in angles of attack of  $0^\circ$  to  $20^\circ$  and load factors of 0g to 3.9g.

Only the windup-turn maneuvers were used to obtain the high angle of attack or high  $C_{N_A}$  data. During the maneuvers, Mach number was kept constant by increasing power, losing altitude, or both. As a result, for the high angle of attack data presented herein, indicated Mach number did not vary by more than 0.01 and dynamic pressure did not vary by more than  $1 \text{ kN/m}^2$  ( $20 \text{ lb/ft}^2$ ).

The flight data for flap deflections of up to  $20^\circ$  were obtained for a dynamic pressure of  $9.6 \text{ kN/m}^2$  ( $200 \text{ lb/ft}^2$ ). Most of the flight data were obtained with the vortex generators installed. However, a few data were obtained at a dynamic pressure of  $9.6 \text{ kN/m}^2$  ( $200 \text{ lb/ft}^2$ ) with the vortex generators removed.

## WIND TUNNEL TESTS

The wind tunnel data presented herein were obtained from tests of a steel pressure model in the NASA Langley Research Center's 8-Foot Transonic Pressure Tunnel (ref. 11). Reynolds number varied from  $2 \times 10^6$  to  $4 \times 10^6$ , based on a mean aerodynamic chord of 0.181 meter (7.12 inches).

The wind tunnel tests were conducted in two phases. In the first phase, the 0.087-scale steel pressure model that was used to determine the structural strength requirements of the airplane was tested. (This was the model used to establish the design cruise condition of the supercritical wing.) The pressure data from these tests were obtained at a high dynamic pressure ( $45 \text{ kN/m}^2$  ( $950 \text{ lb/ft}^2$ )) without the vortex generator and are presented in reference 11.

Minor dissimilarities existed between this wind tunnel model and the full-scale airplane. For example, the model lacked vortex generators, had some wing-surface irregularities, did not incorporate small changes that were made to the inboard surface of the airplane wing, had a different wing-fuselage orientation, and lacked aileron hinge fairings and some small protuberances present on the airplane. These dissimilarities could adversely affect the detailed correlation of wind tunnel and flight pressure distribution data and performance data, but would not be expected to degrade the results of the comparisons presented in this report.

The second phase of the wind tunnel testing was undertaken to provide data obtained at a high dynamic pressure ( $45 \text{ kN/m}^2$  ( $950 \text{ lb/ft}^2$ )) for direct correlation with flight data. The tests were conducted with the 0.087-scale steel pressure model, which was made to accurately represent the full-scale airplane by incorporating the airplane's wing vortex generator, aileron hinge fairings, and other protuberances. Because of the loads at high dynamic pressures, the maximum angle of attack for these tests was limited to approximately  $12^\circ$ .

## RESULTS AND DISCUSSION

### Buffet Sensor Response

A time history of the output of the sensors used to measure the airplane's structural response during airplane buffeting and a corresponding power spectral density plot are presented in figures 4 and 5 for a Mach number of 0.95. The trace for the accelerometer located at the center of gravity is not shown because it was contaminated by noise from the engine inlet duct. For any one sensor, buffet onset would be defined herein as the point at which a definite increase in the unsteady oscillations of the signal was observed. This point is identified on each time history by a dark arrow (fig. 4). The pilot's indication of buffet onset is superimposed on

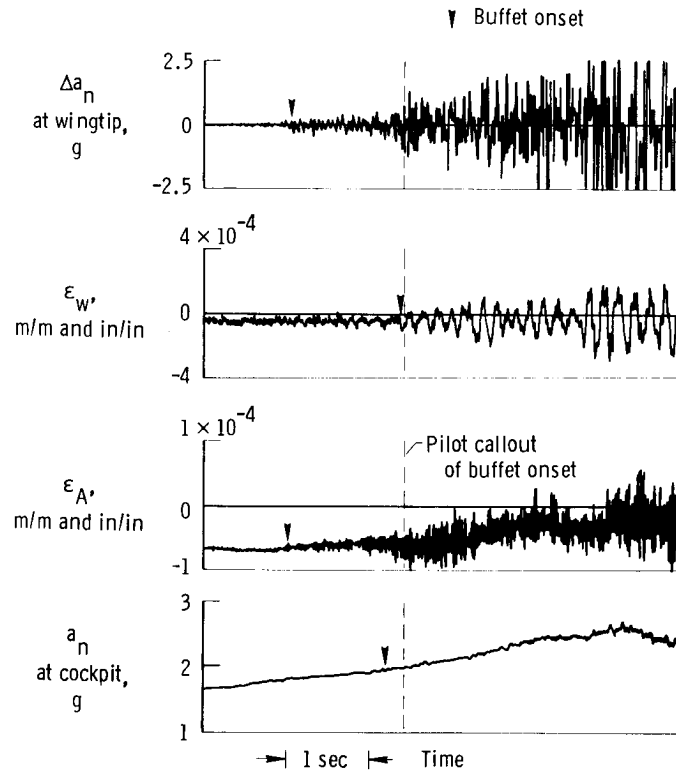
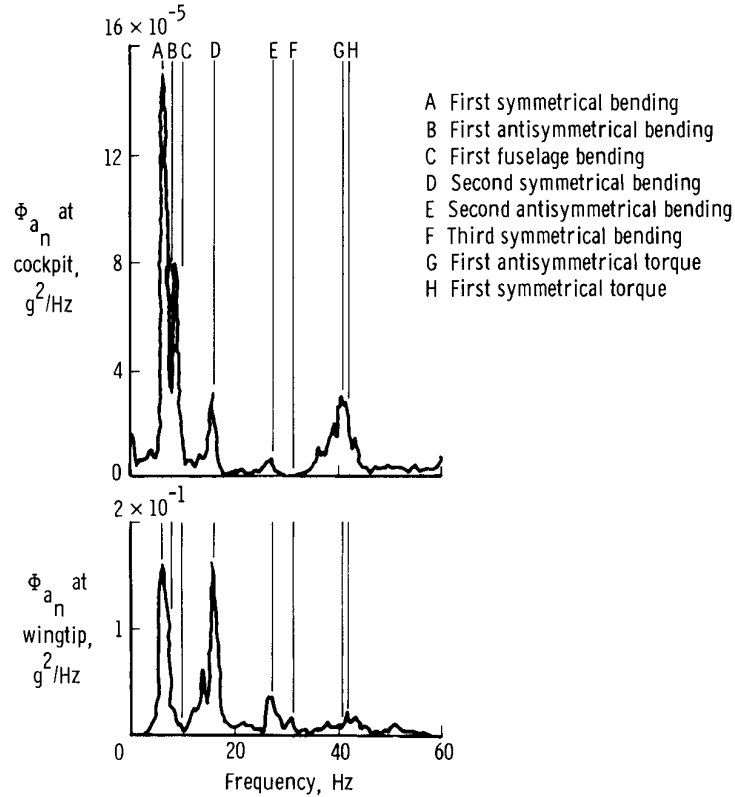


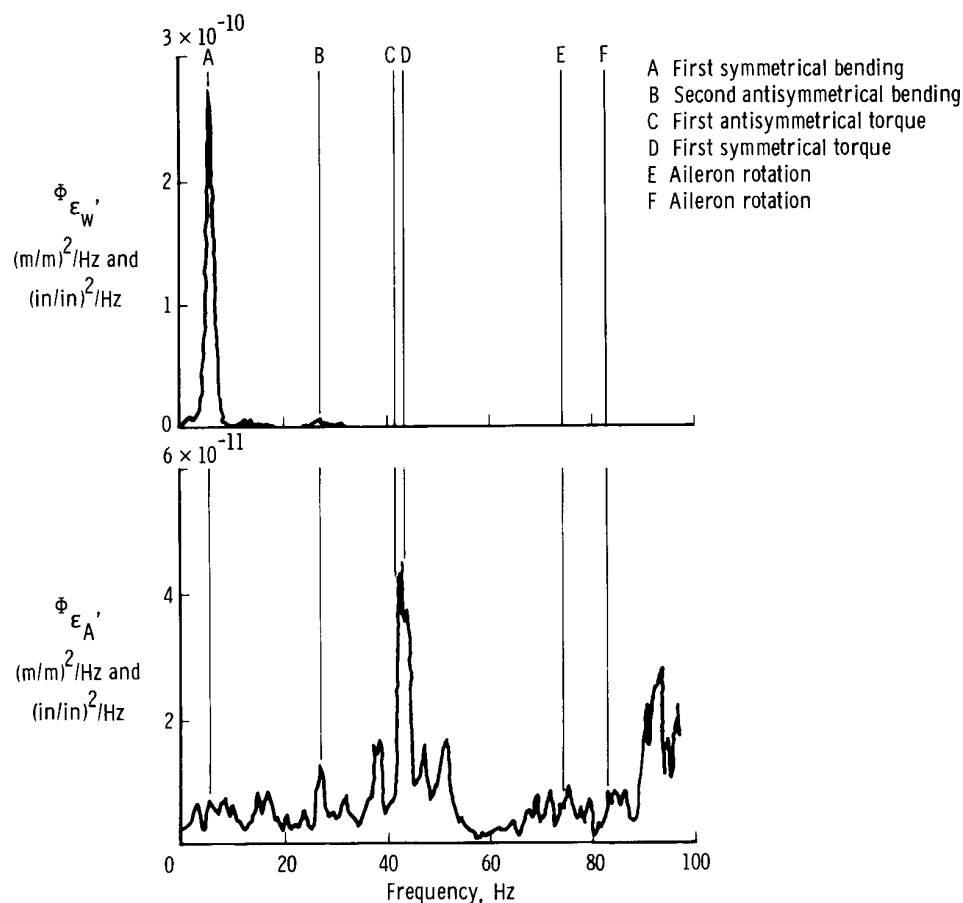
Figure 4. Time histories from sensors used to measure airplane structural response during buffeting for a windup-turn maneuver at Mach 0.95.

the four traces. The various sensors indicate different times for buffet onset and are responsive to different structural frequencies during airplane buffeting (fig. 5). This is to be expected because buffet intensity levels are a direct function of the characteristics of the structure and the sensor location. For example, the cockpit accelerometer is far from the source of the unsteady aerodynamic force that causes the airplane to buffet. In addition, figure 5 shows that the wing-panel bending moment sensor is only sensitive to bending moment frequencies and that the aileron hinge moment sensor is primarily sensitive to torsional and aileron frequencies. The wingtip accelerometer is near the origin of the unsteady aerodynamic forces and is sensitive to both bending and torsional frequencies.



(a) Accelerometers.

Figure 5. Power spectral density.



(b) Strain gages.

Figure 5. Concluded.

### Buffet Onset

The wingtip accelerometer would be expected to give the most accurate measurement of buffet onset because it is near the origin of the unsteady aerodynamic forces. For this reason, the wingtip accelerometer signal was used to determine the buffet onset curve used as a basis for comparison and to measure the structural response of the airplane during buffeting.

The buffet onset boundary based on the response of the wingtip accelerometer is shown in figure 6 for a dynamic pressure of  $9.6 \text{ kN/m}^2$  ( $200 \text{ lb/ft}^2$ ) with the vortex generator installed. The significance of this boundary is the apparent absence of a sharp drop in the buffet boundary, which usually occurs between Mach numbers of 0.80 and 0.90 for conventional subsonic aircraft. When encountered during

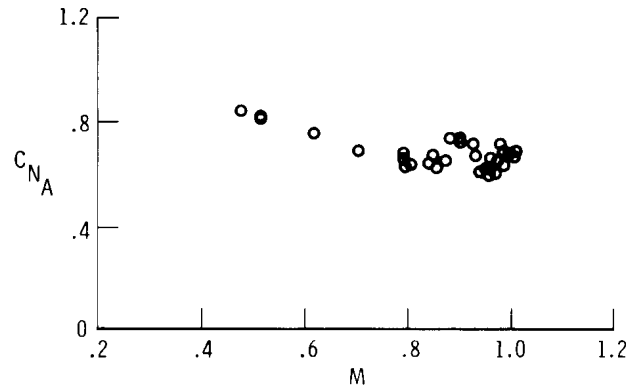


Figure 6. Buffet onset boundary based on response of wingtip accelerometer.

$q = 9.6 \text{ kN/m}^2$  (200 lb/ft<sup>2</sup>); vortex generator installed.

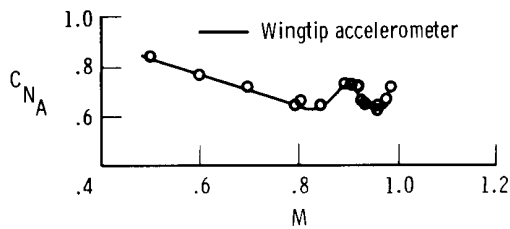
high-speed cruise, this form of buffeting is often termed Mach buffeting. As shown in the figure, the wing does not encounter buffeting at the design cruise normal force coefficient value of 0.40 throughout the Mach range. Although not shown, additional data indicate that neither removal of the vortex generator nor increase in dynamic pressure from  $9.6 \text{ kN/m}^2$  (200 lb/ft<sup>2</sup>) to  $19.2 \text{ kN/m}^2$  (400 lb/ft<sup>2</sup>) affected the buffet onset boundary.

Buffeting is the airplane's structural response to unsteady flow phenomena, which are primarily a function of the airplane's airspeed and attitude. For a constant airspeed and angle of attack,  $C_{N_A}$  varies with weight and center of gravity

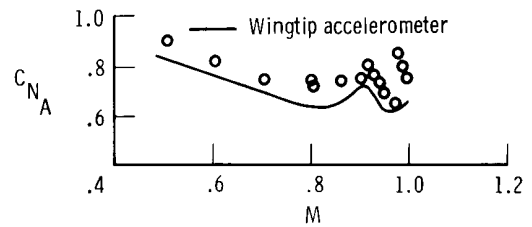
location. Therefore, it would seem desirable to define buffet onset with respect to angle of attack. However, at transonic speeds, the correction to angle of attack with the angle of sideslip vane mounted on the nose boom became nonlinear and random at angles of attack substantially larger than the cruise angle. Because most of the structural response data were obtained from flights with the sideslip vane mounted on the nose boom, the results in the transonic region would appear inconsistent. Therefore, all structural response data in this report are presented with respect to  $C_{N_A}$ . At buffet onset, the maximum error in  $C_{N_A}$  due to weight and center of gravity

variations is 0.02. In addition, the effect of moving the center of gravity from 24 percent of the mean aerodynamic chord to 35 percent of the mean aerodynamic chord is to increase the buffet onset boundary by a  $C_{N_A}$  value of 0.03.

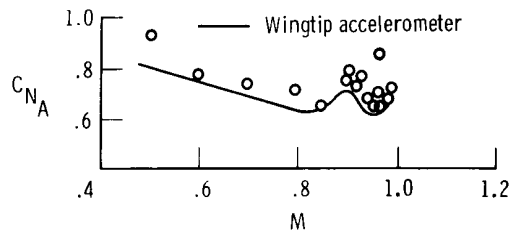
In figure 7, the buffet onset boundaries determined by the sensors other than the wingtip accelerometer are compared with a fairing of the wingtip accelerometer data of figure 6. Of the data from the structural response sensors, the data from the aileron hinge moment gage agree most favorably with that from the wingtip



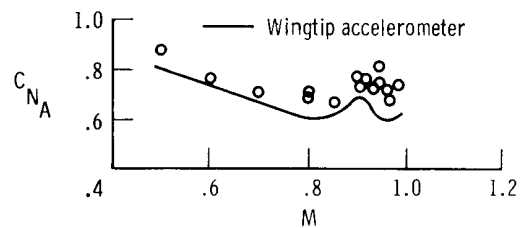
(a) Aileron hinge moment.



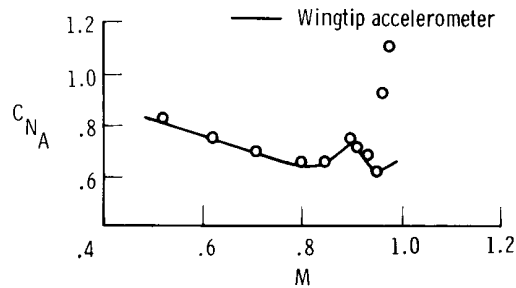
(b) Cockpit accelerometer.



(c) Wing bending moment.



(d) Pilot callout.



(e) Dynamic pressure sensor.

Figure 7. Comparisons of initial responses of various sensors to separated flow.

accelerometer. The other three structural response sensors indicate a slightly higher buffet onset boundary than that indicated by the wingtip accelerometer. The delay in buffet onset indicated by these three sensors is caused by poor sensitivity, location of the sensor on the airplane structure, and susceptibility to background noise. However, in general these sensors indicate the same trends in buffet onset with Mach number. Data from the dynamic pressure sensor are in good agreement with data from the wingtip accelerometer up to Mach 0.95. The reason for the poor agreement above Mach 0.95 is the presence of a local shock wave that shields the sensor from the unsteady separated flow. This effect is discussed in more detail in a later section of this report.

Flight studies of the buffeting characteristics of fighter aircraft (ref. 12) have shown flap deflection to be effective for raising the buffet onset boundary at transonic speeds. Although the flaps on the F-8 supercritical wing airplane were not

designed as maneuvering flaps, it was of interest to examine the effects of flap deflection on the buffet onset boundary. As shown in figure 8, 5° and 10° flap deflections had no apparent effect on the transonic buffet boundary for the data available for comparison. This was expected because the airfoil was already optimized for the transonic Mach range.

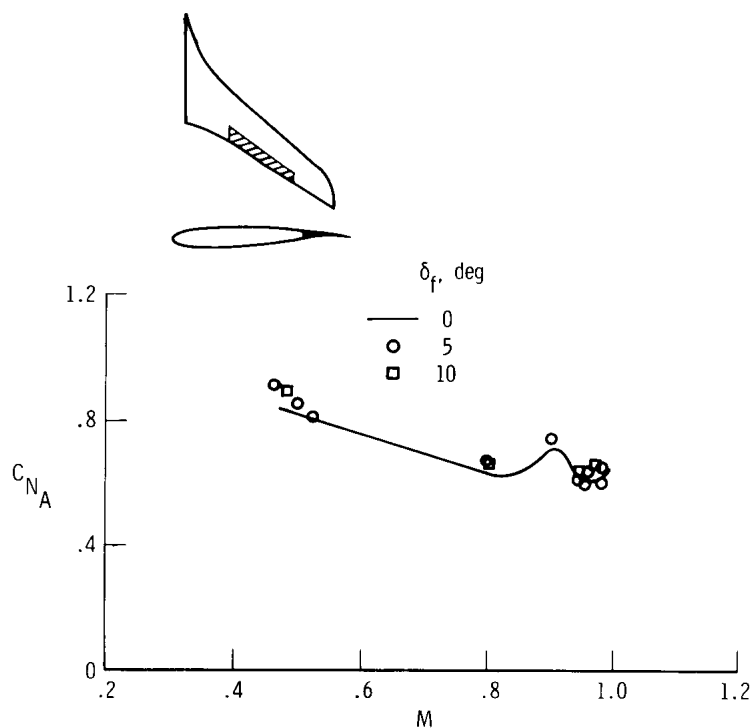


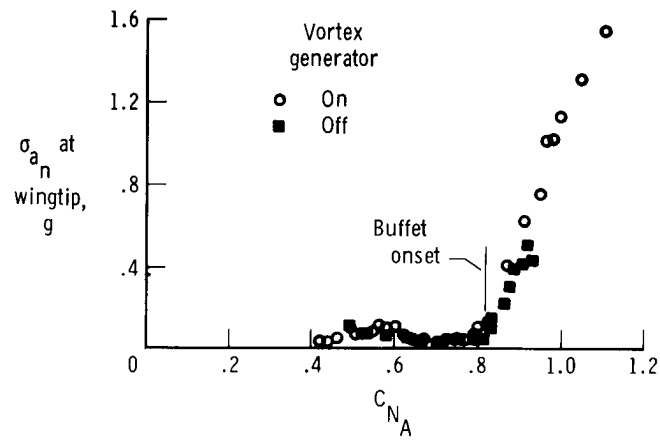
Figure 8. Effect of trailing edge flap deflection on buffet onset boundary.

#### Buffet Intensity

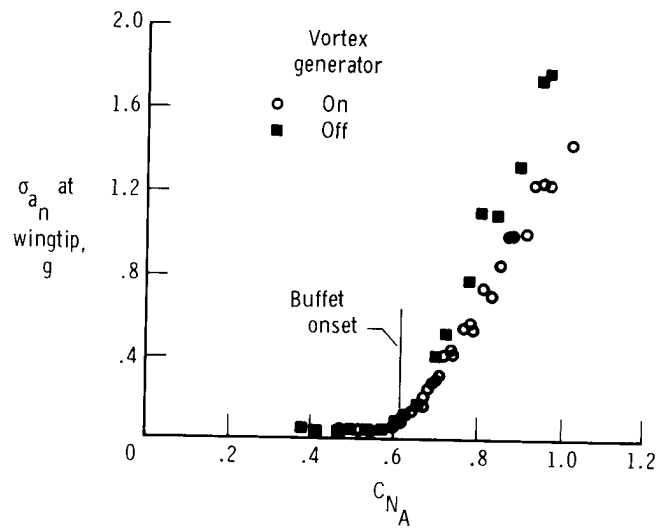
Airplane buffet intensity data from the wingtip accelerometer with the vortex generator on and the vortex generator off are presented in figure 9. The accelerometer data were obtained at a rate of 200 samples per second during windup-turn maneuvers. A root mean square (rms) value was calculated at 0.5-second intervals using 100 data samples.

The buffet intensity curves at Mach 0.50, 0.80, and 0.90 are similar: the buffet intensity level increases rapidly with increase in  $C_{NA}$  immediately following buffet onset. The buffet intensity curves at Mach 0.97 and 0.99 are also similar: there is a period of a slow buildup of buffet intensity following buffet onset. The buffet intensity curve at Mach 0.95 appears to be a transition between the two types of response characteristics.

Previous data indicated that the vortex generator had no effect on the buffet onset boundary. However, the data in figure 9 show a small effect of the vortex generator on the buffet intensity curve at a Mach number of 0.80, which persists to

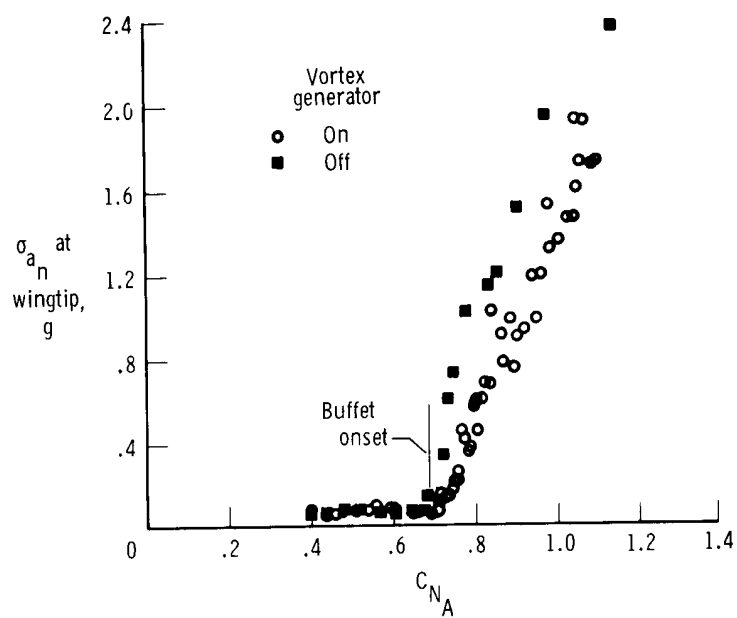


(a) Mach 0.50.

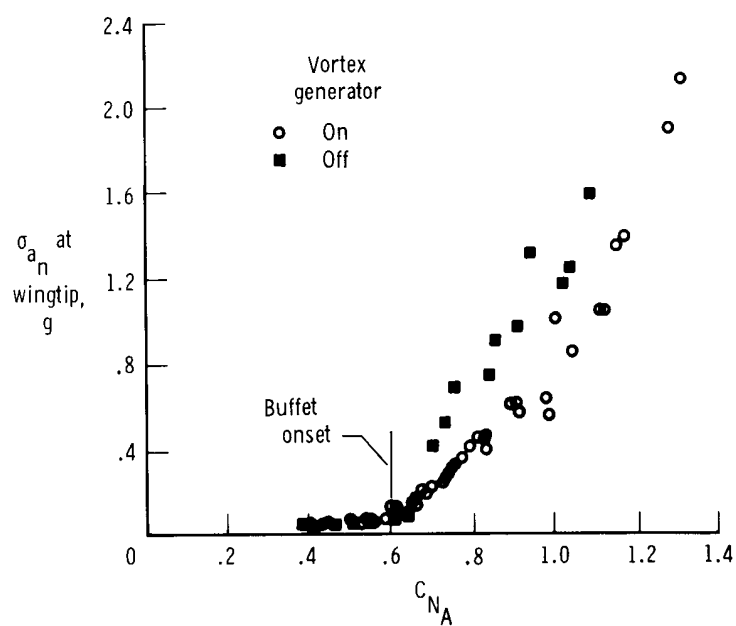


(b) Mach 0.80.

Figure 9. Airplane buffet intensity characteristics.

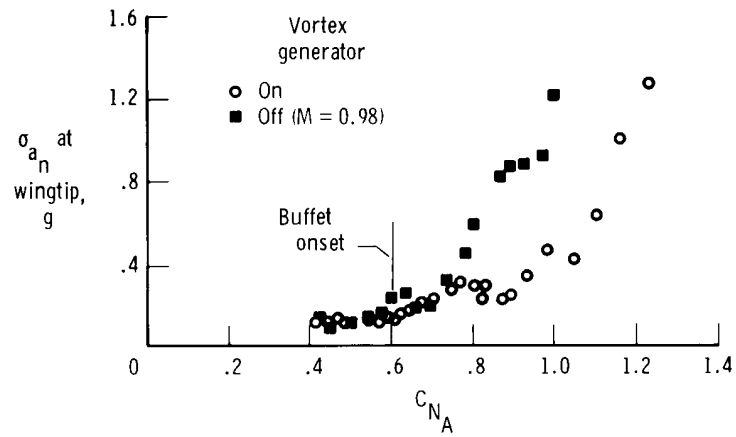


(c) Mach 0.90.

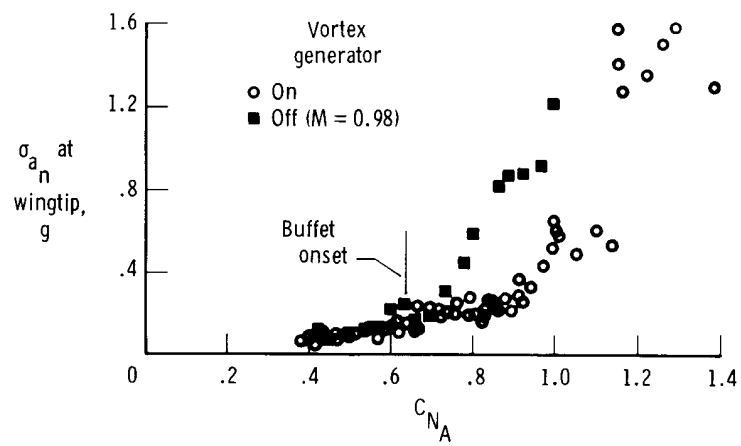


(d) Mach 0.95.

Figure 9. Continued.



(e) Mach 0.97.



(f) Mach 0.99.

Figure 9. Concluded.

a much greater extent at Mach numbers of 0.97 and 0.99. At these higher Mach numbers, the primary effect of the vortex generator is an increase in the increment in  $C_{N_A}$  between buffet onset and the knee in the buffet intensity curve.

The data in figure 9 show that, at a given Mach number, the minimum rms level of buffet before buffet onset tended to remain constant with increasing Mach number up to Mach 0.97, where the minimum intensity level began to increase. In figure 10,

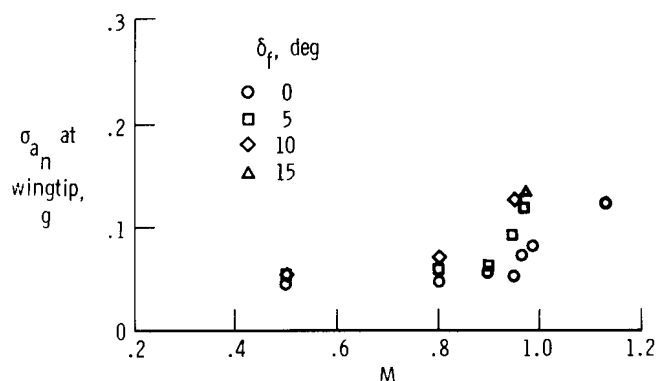


Figure 10. Minimum rms level of buffet intensity before buffet onset, including effect of trailing edge flap deflections.

the minimum rms level of buffet intensity before buffet onset is plotted with Mach number for the clean wing configuration and for several flap-deflected positions. The increase in minimum intensity level above Mach 0.95 may be attributable to a shock on the upper surface of the wing. Deflection of the flaps at Mach 0.95 and above tends to disrupt the flow and thereby increase the minimum level of buffet intensity.

### Flight and Wind Tunnel Correlation

To compare the flight-determined buffet onset boundary with a boundary predicted from wind tunnel tests, the change in upper surface pressure coefficient near the trailing edge with change in angle of attack was investigated. The divergence of the upper surface trailing edge pressure could be related to buffet onset for separation that started at the trailing edge and spread rapidly forward. The data with and without the vortex generator are presented in figure 11. Data are presented only for the four outboard rows of upper surface trailing pressure because rows 1 and 2 do not exhibit divergence over the range of angle of attack presented. A few flight data were obtained and these data are presented to illustrate the ability of the wind tunnel to represent the general flow characteristics of the flight-tested supercritical wing.

The flight data and wind tunnel data are in general agreement at all Mach numbers except Mach 0.90, where the flight data show that, at an angle of attack

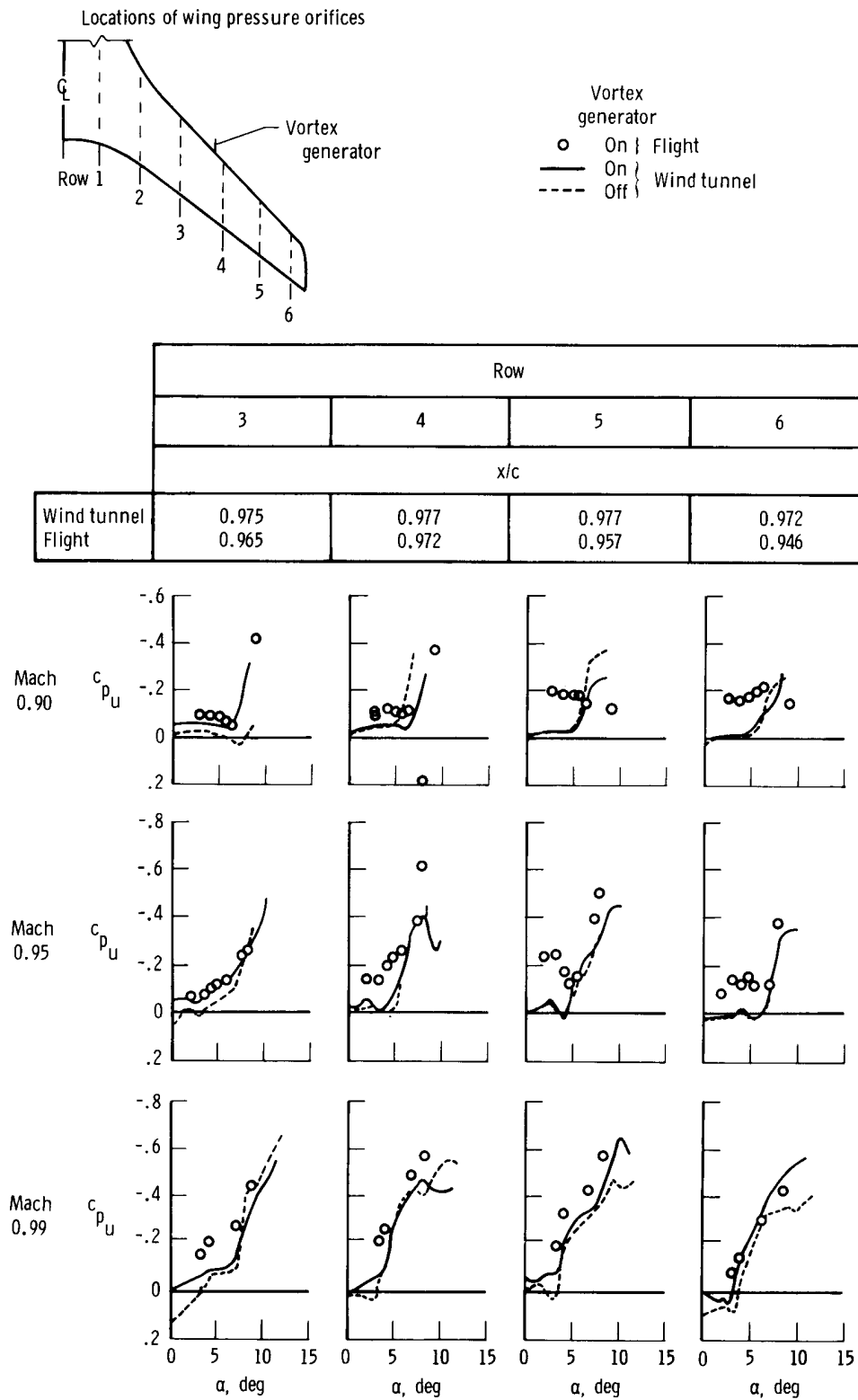


Figure 11. Flight and wind tunnel upper surface pressures near trailing edge.

of approximately  $9^\circ$ , the two outboard rows maintain a pressure recovery at the trailing edge. There is no significant difference between the data with and without the vortex generator.

If the point at which the trailing edge pressures diverge is representative of buffet onset, the data in figure 11 suggest that the vortex generator should not affect the buffet onset boundary. In addition, the data show that the trailing edge pressures of rows 4, 5, and 6 are more sensitive to the initial flow separation than those of rows 1, 2, and 3. Consequently, the three outboard rows of trailing edge pressures were used to predict the buffet onset boundary from wind tunnel data.

In figure 12, the flight-determined buffet boundary is compared with the predicted wind tunnel buffet boundary, which is derived from the trailing edge

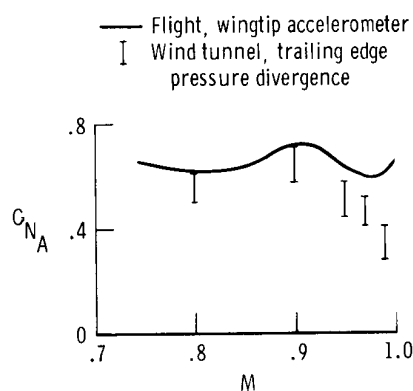


Figure 12. Comparison of flight buffet onset boundary with wind tunnel indicator.

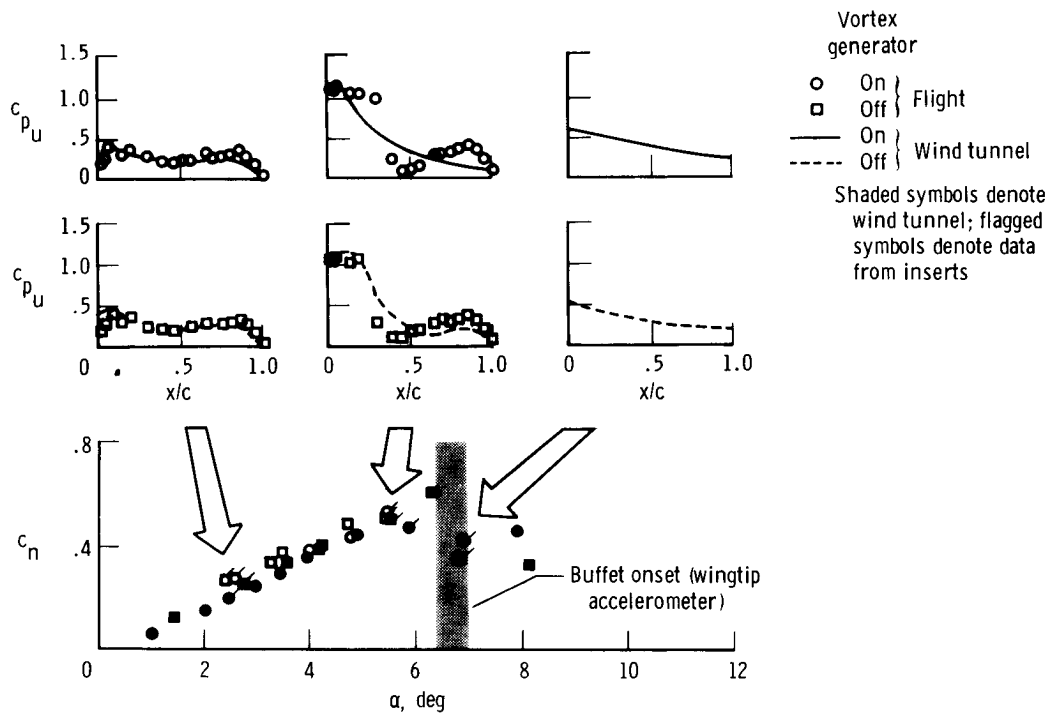
pressure divergence. The lower bound of the symbol representing the wind tunnel predictions indicates the initial divergence of any of the three outboard rows of trailing edge pressures. The upper bound represents the divergence of all three outboard rows of trailing edge pressures.

At Mach 0.80 and 0.90, the wind tunnel values of  $C_{NA}$  for the upper bound of the trailing edge pressure divergence agree fairly well with the flight data. In fact, the trends in buffet onset  $C_{NA}$  with Mach number are similar for flight and wind tunnel data up to Mach 0.97. From Mach 0.97 to 0.99, the buffet boundary for the wind tunnel data drops sharply. It is hypothesized that the two boundaries are different because the trailing edge pressure divergence represents the beginning

of an aerodynamic disturbance or forcing function, whereas the flight-determined buffet onset data represent the initial measurable response of the wing to the aerodynamic disturbance.

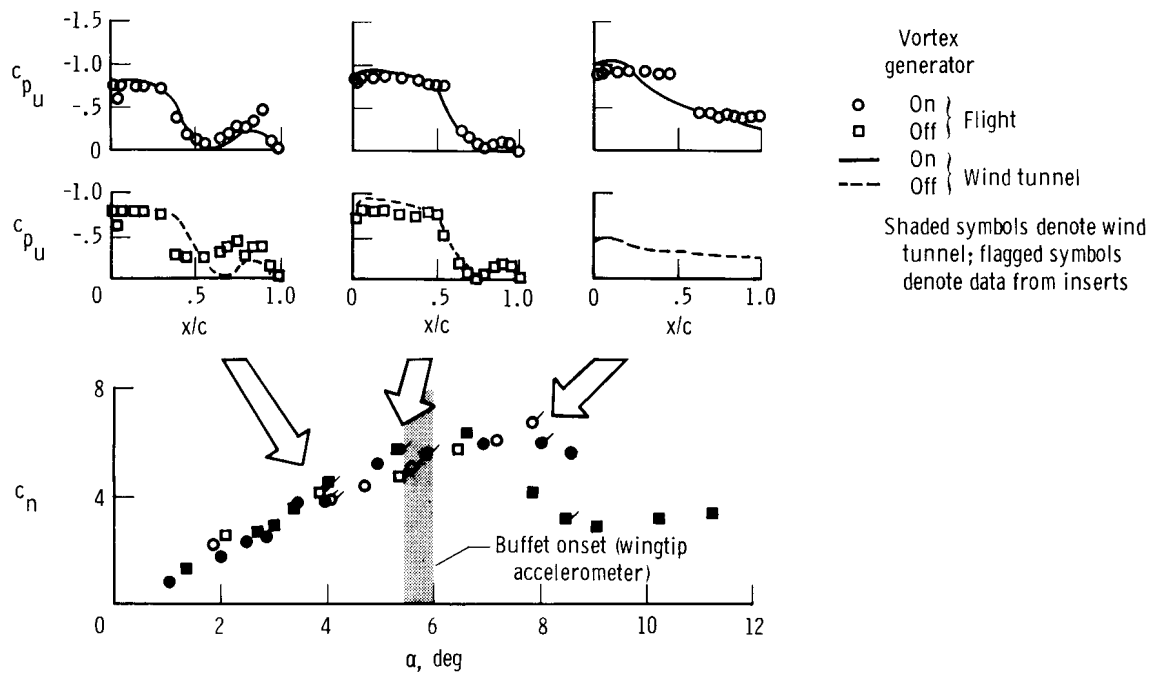
### Flow Studies

In an attempt to understand the difference between the trailing edge pressure divergence boundary and the initial structural response boundary, the characteristics of supercritical flow near the cruise Mach number were examined. Figure 13 presents some wind tunnel-integrated and flight-integrated pressure data for the outboard wing panel at Mach numbers of 0.90, 0.95, and 0.99. Data at Mach numbers of 0.50 and 0.80 are not presented because the behavior of the flow at Mach 0.90 is representative of the flow at the lower subsonic Mach numbers. The plots inserted

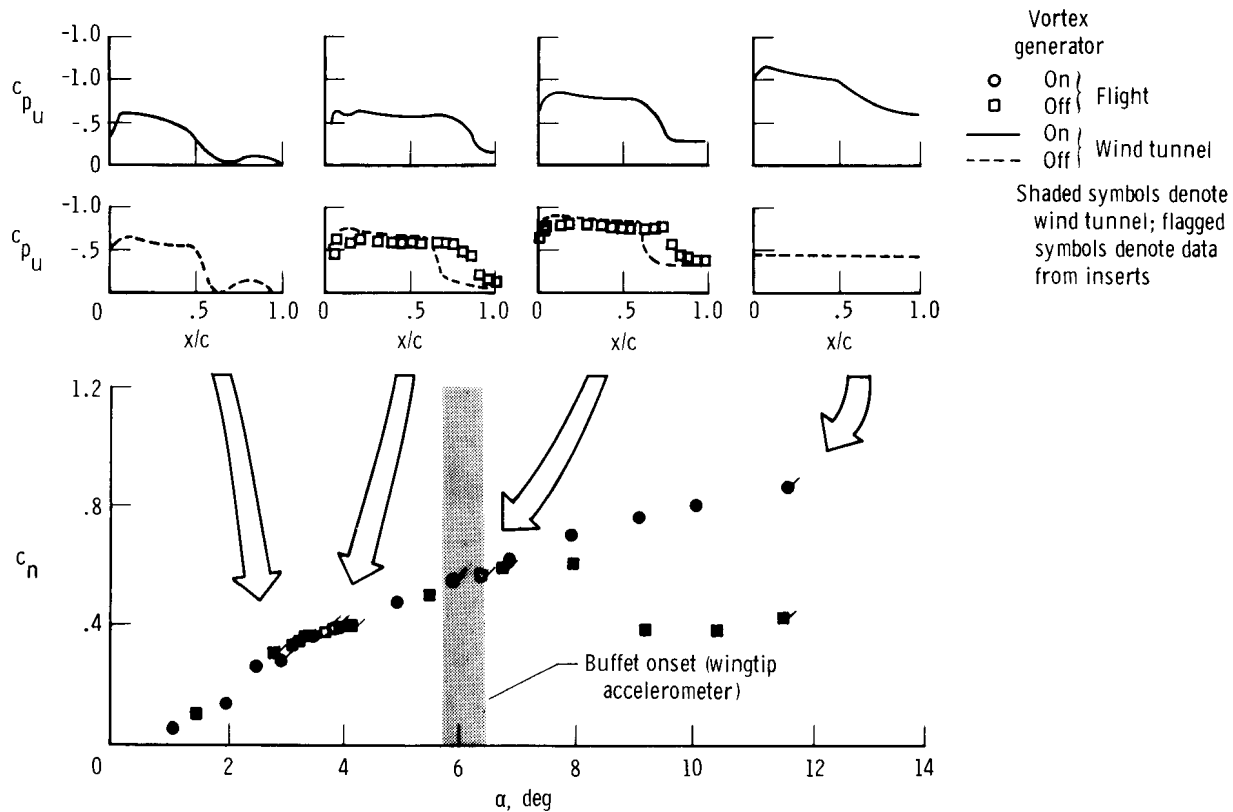


(a) Mach 0.90.

Figure 13. Effect of supercritical wing flow characteristics on outboard wing panel (row 6).



(b) Mach 0.95.



(c) Mach 0.99.

Figure 13. Concluded.

above the normal force curve for the sixth row of upper surface pressures are the chordwise pressure distributions that correspond to the flagged symbols. Both flight and wind tunnel pressure data are presented. However, the flight data are restricted to the lower angles of attack and in some cases do not penetrate the buffet onset boundary. The pressure data are also presented for tests with the vortex generator on and off.

At Mach 0.90, the flow on the upper surface is attached at angles of attack of  $2.5^\circ$  and  $5.5^\circ$ . Buffet onset (as determined from the wingtip accelerometer) occurs at the break in the section normal force curve, at which point the flow on the upper surface of the outer wing is largely separated. There is good agreement between the flight and wind tunnel data, and there is no significant difference between the data with the vortex generator on and the data with the vortex generator off.

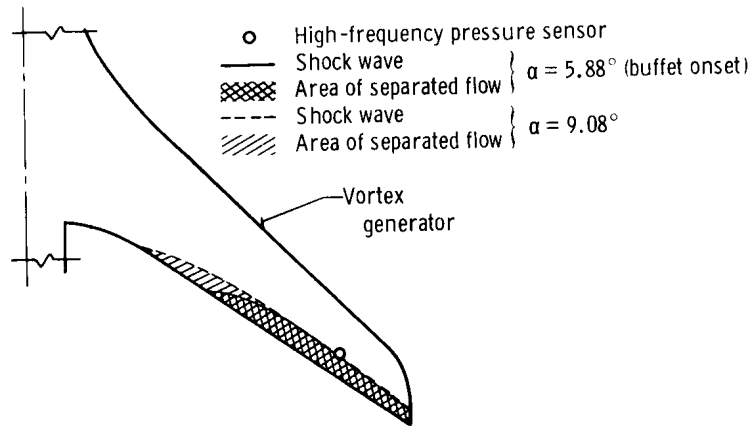
At Mach 0.95, the flow over the upper surface is attached at angles of attack of  $4.0^\circ$  and  $5.5^\circ$ . Buffet onset appears to occur before the severe break in the section normal force curve. Beyond buffet onset, at an angle of attack of  $8^\circ$ , the upper surface chordwise pressure distributions show a distinct effect of the vortex generator. The wind tunnel data without the vortex generator show that nearly all of the flow on the upper surface is separated. The flight and wind tunnel data with the vortex generator show that the separated flow region is restricted to the area behind the shock. At this Mach number, the effects of supercritical flow and the vortex generator begin to appear.

At Mach 0.99, the section normal force curve is characterized by two distinct linear ranges. In the initial linear range (an angle of attack of less than  $3.5^\circ$ ), the flow over the upper surface is attached. As the angle of attack approaches  $4.0^\circ$ , the shock on the upper surface begins to move rearward, the trailing edge pressure begins to diverge, a small region of separated flow is identified behind the shock, and a mild break occurs in the normal force coefficient curve. The second linear range in the normal force curve is characterized by a region of separated flow that is restricted to the area behind the shock. At an angle of attack of approximately  $6^\circ$ , as the shock on the upper surface moves forward and increases the area of separated flow, buffet onset is identified from the wingtip accelerometer data. Up to this point, there is no difference in the behavior of the flow with the vortex generator on or off. At angles of attack greater than  $8^\circ$ , wind tunnel data without the vortex generator show separated flow over the entire chord. Corresponding data with the vortex generator show the presence of a shock at an angle of attack of  $11.5^\circ$ , with the separated flow restricted to the area behind the shock. The effects of the underwing vortex generator on the flow characteristics of the F-8 supercritical wing airplane are discussed in more detail in reference 7.

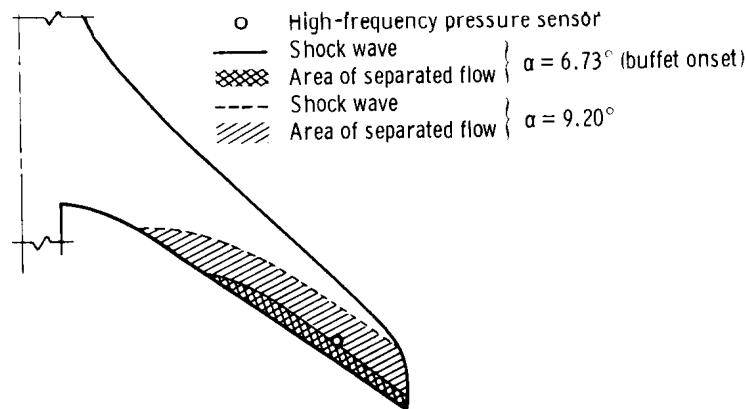
Figure 13 shows that at the higher Mach numbers the shock confines the initial separated flow region to an area sufficiently small that the structural sensors do not respond until  $C_{N_A}$ , or  $\alpha$ , reaches a value much larger than that for the trailing edge pressure divergence. Therefore, above Mach 0.90, the trailing edge pressure

divergence does not appear to be a good indicator of buffet onset as defined by the structural response and, conversely, the buffet onset from structural response is not an indication of the initial flow separation. However, at Mach 0.90 and below, the upper surface shock does not affect the separated flow region. Therefore, at the lower Mach numbers, the trailing edge pressure divergence boundary shows good agreement with the buffet onset boundary determined from the structural sensor data.

The extent of the separated flow on the wing at the buffet onset defined by the wingtip accelerometer, including the effect of the vortex generator, is shown in figure 14 for a Mach number of 0.99. The figure shows the shock locations as



(a) Vortex generator on.

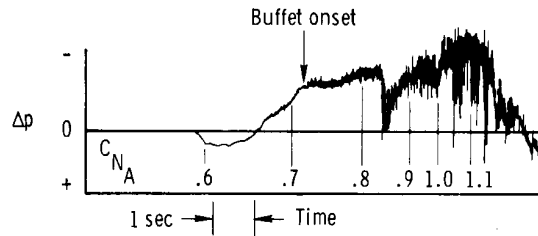


(b) Vortex generator off.

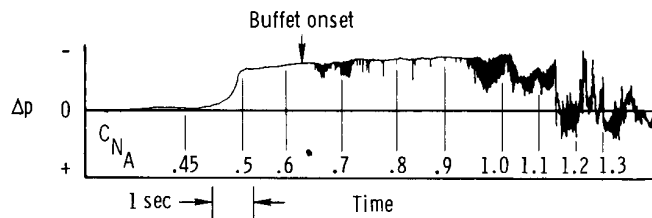
Figure 14. Wing flow separation at buffet onset and higher angles of attack with vortex generator on and off. Mach 0.99.

determined from wind tunnel pressure data. The flow behind the shock is separated. At buffet onset, which occurs at an angle of attack of approximately  $6^\circ$ , an appreciable area of separated flow exists. The extent of the separated flow is approximately the same for the data with the vortex generator on and off. At an angle of attack of approximately  $9^\circ$ , the data with the vortex generator off show a significant increase in separated flow whereas the data with the vortex generator on show only a small increase in separated flow. As expected, the data with the vortex generator off produce a more rapid increase in buffet intensity with increase in  $C_{N_A}$  or angle of attack. This effect is shown in the buffet intensity data presented in figure 9.

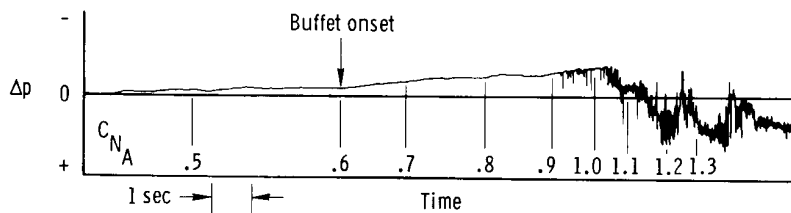
As shown in figure 14, a high-frequency pressure sensor was installed near the shock location at the design cruise condition. This sensor was useful in the study of the pressure fluctuations associated with the movement of the shock wave. Figure 15 shows time histories of pressure fluctuations at Mach numbers of 0.90,



(a)  $M = 0.90$ .



(b)  $M = 0.95$ .



(c)  $M = 0.98$ .

Figure 15. Response of high frequency pressure sensor with vortex generator installed.

0.95, and 0.98 with the vortex generator on. Corresponding  $C_{N_A}$  values are tabulated below each time history. At Mach 0.90 there is no evidence of a shock passing over the sensor when the values of  $C_{N_A}$  increase, and the buffet onset indicated by the pressure fluctuations agrees with that indicated by the wingtip accelerometer (fig. 7). At Mach 0.95 and a  $C_{N_A}$  of approximately 0.65, the shock begins to fluctuate behind and over the sensor until a  $C_{N_A}$  of approximately 1.0 is attained when the shock begins to pass forward of the sensor. The flow behind the shock is separated, as shown by the large pressure fluctuations at  $C_{N_A}$  values of 1.2 and greater. The buffet onset defined by the wingtip accelerometer occurs slightly before the pressure sensor is excited. The important difference at Mach 0.98 is that the shock is to the rear of the pressure sensor, as shown in figure 14. The shock approaches the sensor at a  $C_{N_A}$  of approximately 0.9. The buffet onset defined by the wingtip accelerometer occurs at a  $C_{N_A}$  of 0.61, but the smoothness of the pressure sensor data between the  $C_{N_A}$  values of 0.6 and 0.9 indicates that the shock restricts the propagation of the separated flow region.

#### CONCLUDING REMARKS

The buffet characteristics of the F-8 supercritical wing airplane were investigated using various structural response sensors and a dynamic pressure sensor. The data from the structural response sensors were correlated to flight and wind tunnel pressure data in an attempt to relate the supercritical flow characteristics to the airplane buffeting as measured by the structural sensors.

The structural response of the airplane was best represented by the wingtip accelerometer because of its proximity to the separated flow and its response to the various structural modes excited by the unsteady flow. Two structural response modes were identified by the wingtip accelerometer data for the F-8 supercritical wing airplane: one that is not affected by an upper surface shock and one that is affected by an upper surface shock. The former mode occurred at Mach 0.90 and below and was characterized by a rapid increase in buffet intensity immediately after buffet onset. Wind tunnel and flight pressure data indicated that the rapid increase in buffet intensity could be related to the extensive and rapid propagation of separated flow over the outer wing panel. The latter structural response mode occurred from Mach 0.95 to Mach 0.99 and was characterized by a period of a slow increase in buffet intensity immediately after buffet onset and before the rapid increase in buffet intensity. The wind tunnel and flight pressure data indicated that the period of slow increase in buffet intensity is due to the presence of an upper surface shock, located near the trailing edge, which delays the rapid propagation of separated flow over the outer wing panel, thereby delaying the rapid increase in buffet intensity.

The vortex generator had little effect on the buffet or flow characteristics at Mach 0.90 and below. However, at Mach 0.95 to 0.99, the vortex generator stabilized the upper surface shock, thereby significantly delaying the rapid increase in buffet intensity with increase in airplane normal force coefficient. The vortex generator did not affect the buffet onset boundary as determined from the wingtip accelerometer data.

The buffet onset boundary from flight showed a higher-than-cruise value of airplane normal force coefficient throughout the Mach range, without the sharp drop that generally occurs at the higher transonic speeds.

Moderate deflections of the trailing edge flaps had no discernible effect on the transonic buffet boundary.

At Mach 0.90 and below, the wind tunnel trailing edge pressure divergence boundary is in agreement with the flight-determined buffet boundary. Above Mach 0.90, the wind tunnel data produced a considerably lower boundary, which suggests that for the supercritical wing, the trailing edge pressure divergence is not a valid indication of buffet onset as measured by structural response sensors.

*Dryden Flight Research Center  
National Aeronautics and Space Administration  
Edwards, Calif., September 30, 1976*

## REFERENCES

1. Supercritical Wing Technology—A Progress Report on Flight Evaluations. NASA SP-301, 1972.
2. DeAngelis, V. M.: Wing Panel Loads and Aileron Hinge Moments Measured in Flight on the F-8 Supercritical Wing Airplane Including Correlations With Wind Tunnel Data. NASA TM X-3098, 1974.
3. Pyle, Jon S.; and Steers, Louis L.: Flight-Determined Lift and Drag Characteristics of an F-8 Airplane Modified With a Supercritical Wing With Comparisons to Wind-Tunnel Results. NASA TM X-3250, 1975.
4. Montoya, Lawrence C.; and Banner, Richard D.: F-8 Supercritical Wing Flight Pressure, Boundary-Layer, and Wake Measurements and Comparisons With Wind Tunnel Data. NASA TM X-3544, 1977.
5. Mechtly, E. A.: The International System of Units—Physical Constants and Conversion Factors. Second Revision. NASA SP-7012, 1973.
6. Harris, Charles D.; and Bartlett, Dennis W.: Tabulated Pressure Measurements on a NASA Supercritical-Wing Research Airplane Model With and Without Fuselage Area-Rule Additions at Mach 0.25 to 1.00. NASA TM X-2634, 1972.
7. Harris, Charles D.; and Bartlett, Dennis W.: Wind-Tunnel Investigation of Effects of Underwing Leading-Edge Vortex Generators on a Supercritical-Wing Research Airplane Configuration. NASA TM X-2471, 1972.
8. Kelly, Thomas C.; and Whitcomb, Richard T.: Evolution of the F-8 Supercritical Wing Configuration. Supercritical Wing Technology—A Progress Report on Flight Evaluations. NASA SP-301, 1972, pp. 35-47.
9. Andrews, William H.: Status of the F-8 Supercritical Wing Program. Supercritical Wing Technology—A Progress Report on Flight Evaluations. NASA SP-301, 1972, pp. 49-58.
10. Pyle, Jon S.: Preliminary Lift and Drag Characteristics of the F-8 Supercritical Wing Airplane. Supercritical Wing Technology—A Progress Report on Flight Evaluations. NASA SP-301, 1972, pp. 59-70.
11. Harris, Charles D.: Wind-Tunnel Measurements of Aerodynamic Load Distribution on an NASA Supercritical-Wing Research Airplane Configuration. NASA TM X-2469, 1972.
12. Monaghan, Richard C.; and Friend, Edward L.: Effects of Flaps on Buffet Characteristics and Wing-Rock Onset of an F-8C Airplane at Subsonic and Transonic Speeds. NASA TM X-2873, 1973.

|  |  |  |  |  |  |
|--|--|--|--|--|--|
| 1. Report No.<br>NASA TM-56049   |  | 2. Government Accession No.                          |  | 3. Recipient's Catalog No.   |  |
| 4. Title and Subtitle<br>BUFFET CHARACTERISTICS OF THE F-8 SUPERCRITICAL<br>WING AIRPLANE  |  |  |  | 5. Report Date<br>September 1977   |  |
|  |  |  |  | 6. Performing Organization Code  |  |
| 7. Author(s)<br>V. Michael DeAngelis and Richard C. Monaghan   |  |  |  | 8. Performing Organization Report No.<br>H-945                                   |  |
| 9. Performing Organization Name and Address<br>NASA Dryden Flight Research Center<br>P.O. Box 273<br>Edwards, California 93523   |  |  |  | 10. Work Unit No.<br>505-02-23   |  |
|  |  |  |  | 11. Contract or Grant No.  |  |
|  |  |  |  | 13. Type of Report and Period Covered<br>Technical Memorandum                    |  |
| 12. Sponsoring Agency Name and Address<br>National Aeronautics and Space Administration<br>Washington, D.C. 20546  |  |  |  | 14. Sponsoring Agency Code   |  |
|  |  |  |  |  |  |
| 15. Supplementary Notes  |  |  |  |  |  |
| 16. Abstract<br><br><p style="text-align: center;">The buffet characteristics of the F-8 supercritical wing airplane were investigated. Wing structural response was used to determine the buffet characteristics of the wing and these characteristics are compared with wind tunnel model data and the wing flow characteristics at transonic speeds. The wingtip accelerometer was used to determine the buffet onset boundary and to measure the buffet intensity characteristics of the airplane. The effects of moderate trailing edge flap deflections on the buffet onset boundary are presented. The supercritical wing flow characteristics were determined from wind tunnel and flight static pressure measurements and from a dynamic pressure sensor mounted on the flight test airplane in the vicinity of the shock wave that formed on the upper surface of the wing at transonic speeds. The comparison of the airplane's structural response data to the supercritical flow characteristics includes the effects of a leading edge vortex generator.</p> |  |  |  |  |  |
| 17. Key Words (Suggested by Author(s))<br><br>Supercritical wing<br>Buffet<br>Flow separation<br>Transonic flight testing  |  |  |  | 18. Distribution Statement<br><br>Unclassified—Unlimited<br><br><br>Category: 02 |  |
| 19. Security Classif. (of this report)<br>Unclassified   |  | 20. Security Classif. (of this page)<br>Unclassified |  | 21. No. of Pages<br>28   |  |
|  |  |  |  | 22. Price*<br>\$3.75   |  |